Nanoscale

Accepted Manuscript

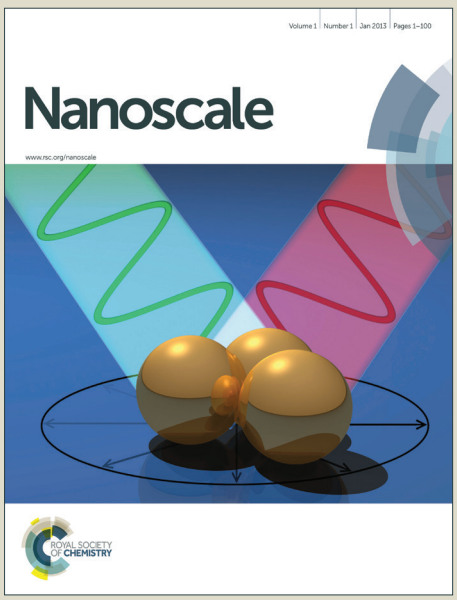

ROYAL SOCIETY OF CHEMISTRY

www.rsc.org/nanoscale

NANOSCALE

PAPER

Improvement of polypyrrole nanowire device by plasmonic space charge generation: high photocurrent and wide spectral response by Ag nanoparticle decoration

Received 00th January 20xx,
Accepted 00th January 20xx

DOI: 10.1039/x0xx00000x

www.rsc.org/

S.-H. Lee[a], J. Bae[b], S. W. Lee[b] and J.-W. Jang*[,a]

In this study, improvement of opto-electronic properties of non-single crystallized nanowire devices with space charges generated by localized surface plasmon resonance (LSPR) is demonstrated. Photocurrent and spectral response of single polypyrrole (PPy) nanowire (NW) devices are increased by electrostatically attached Ag nanoparticles (Ag NPs). To take advantage of plasmon–exciton coupling in photocurrent of the device, 80 nm of Ag NPs (454 nm = λ_{max}) were chosen for matching maximum absorption with PPy NWs (442 nm = λ_{max}). Photocurrent density is remarkably improved, up to 25.3 times (2530%), by the Ag NPs decoration onto the PPy NW (PPy_{AgNPs} NW) under blue light (λ = 425–475 nm) illumination. In addition, the PPy_{AgNPs} NW shows photocurrent decay time twice that of PPy NW, as well as improved spectral response of photocurrent. The improved photocurrent efficiency, decay time, and spectral response are resulted from space charges generated by LSPR of Ag NPs. Furthermore, increasing exponent (*m*) of photocurrent ($J_{PC} \sim V^m$) and finite-differential time domain (FDTD) simulation straightforwardly indicates relatively large plasmonic space charge generation under blue light illumination. These results prove that performance of non-single crystallized polymer nanowire devices can be also improved by plasmonic enhancement.

Introduction

Hybrid nanostructures have attracted attention due to many novel properties that are lacking in any one material. Among hybrid nanostructures, semiconductor nanowires (NWs) with metal nanomaterials have been more exploited because metal and semiconductor have different properties that, in combination, result in unique electrical and optical properties.[1-4] Localized surface plasmon resonance (LSPR), which is one of novel properties of metal nanoparticles (NPs), has been used as a good strategy for increasing photovoltaic performance in semiconductor NW; strong scattering and surface-absorption result from LSPR of the metal NPs on photovoltaic semiconductor.[5,6] In the results, improved solar energy conversion and enhanced photocurrent are obtained near the interface of the device.[5,6] Another unique property in metal NPs-attached semiconductor NW (NW_{Semi}) systems is polarization-dependent performance due to one-dimensional geometry of NW.[6] In detail, three different roles of the metal NPs in enhancing opto-electronic properties of the metal NPs-attached NW_{Semi} system have been identified: (i) magnified local electrical field (*E*-field) by LSPR can effectively separate photo-generated electron–hole pairs (excitons),[7,8] (ii) excited electrons by LSPR can inject into the NW_{Semi} (hot-electron generation and injection),[9,10] and (iii) photon absorption in NW_{Semi} can be intensified by resonance photon scattering or plasmon resonance energy transfer.[5] In order to maximize the plasmonic enhancement in the metal NPs – NW_{Semi} system, bandgap matching or overlapping between LSPR of the metal NPs and absorption of the NW_{Semi} have been tried. However, it is still under debating on the mechanism about enhancing photocurrent and photocatalytic effect under light illumination at interface of the metal NPs – NW_{Semi} system; for example. Pu *et al.*[11] reported that the matching of the Au LSPR wavelength with band-gap of TiO_2 can boost hot-electron injection and improve photoactivity in Au nanostructures decorated TiO_2 NW. However, instead of hot-electron injection, charge separation was also directly observed by using Kelvin probe force microscopy in Au NPs on TiO_2 nanotube as a key factor of enhancing photocatalytic effect.[12] Furthermore, complementary reports on the role of light-induced hot-electron in NW_{Semi} devices have been demonstrated. Pescaglini *et al.*[13] reported that photocurrent increases about 20-fold by injection of hot-electrons in Au nanorods-ZnO NW hybrid systems. They also claim that the photocurrent rapidly decays because the injected hot-electrons are not related with surface defect-sites on the ZnO NW. On the other hand, hot-electron injection associated with surface defect-sites also has been

[a] *Department of Physics, Pukyong National University, Busan 608-737, Republic of Korea, E-mail: jjang@pknu.ac.kr*
[b] *Address here. School of Display & Chemical Engineering, Yeungnam University, Gyeongsan, 712-749, Republic of Korea*

†Electronic Supplementary Information (ESI) available: SEM image of crude PPy NWs and TEM image of PPy NW. Fabrication of PPy NW and PPy_{AgNPs} NW devices. EDS analysis of PPy_{AgNPs} NW device. Control experiment of electrostatic Ag NPs decoration on PPy NWs. Ohmic behavior of PPy NW and PPy_{AgNPs} NW devices in low voltage region. Vector plots of *E*-field at interface between Ag NP and PPy NW. FDTD simulating absorption spectra. See DOI: 10.1039/x0xx00000x

reported; Lu, *et al.*[3] reported enhanced photocurrent gain and spectral response of quantum dots (QDs)-attached SnO_2 NW device. Due to band bending at the interface between the QDs and the SnO_2 NW, space charges are generated at the interface when hot-electrons are injected therein. Extending space charge region by hot-electron injection can be regarded similarly to increasing defect-sites at the interface, as transport of charge carriers is also hampered by defect-sites. The enhanced photocurrent gain and spectral response are explained, respectively, by accelerating separation of excitons with enhanced local *E*-field in the space charge region and bandgap mismatching (different wavelengths in maximum absorption) between the QDs and the SnO_2 NW. Interestingly, the non-rapid decay is observed in hot-electron injected photocurrent of the QDs-attached SnO_2 NW devices. Similarly to the QDs-attached SnO_2 NW device, it was reported that extended space charge region and enhanced photocurrent are also available by metal NP (Au NP) decoration on a SnO_2 NW device.[14] In this case, increase of the barrier height at the interface results from differences in work-functions of Au NPs and SnO_2 NW; therefore, space charge region is extended by increasing the barrier height at the interface.[14]

Even though space charges in NW_{Semi} devices operate similarly to defect-sites, space charges can enhance opto-electric properties of NW_{Semi} devices. Space charges are favorably built-up in conducting polymers due to their non-single crystallinity. Therefore, the aforementioned plasmonic approach to generating space charges at the interface can be applied to conducting polymer NW in order to improve opto-electronic properties; however, plasmonic enhancement in photocurrent of non-single crystallized polymer NW devices has not been reported yet. In addition, most plasmonic enhancement and hot-electron studies[3,4,11-13] using NPs-attached NW_{Semi} have been conducted on *n*-type NW_{Semi}. Because comparable opto-electronic study using *p*-type NW_{Semi} is desirable to acquire better understandings on the mechanism of enhancing photocurrent and photoactivity, metal NPs-decorated *p*-type conducting polymer NW will be a good test bed for a comparable study.

In this study, it is demonstrated that photocurrent and spectral response are remarkably improved by LSPR-generated space charges in Ag NPs-attached individual polypyrrole (PPy) NW device. In particular, we complementally prove the space charge generation by LSPR of Ag NPs by means of characterizing current–voltage (*J*–V) dependence and finite-differential time domain (FDTD) simulation on the NW devices, respectively. In the result, improvement of photocurrent and spectral response of the device can be attributed by space charge enhancing local *E*-field as well as matching maximum absorption spectra between Ag NPs and PPy NW (plasmon-exciton coupling such as plasmon resonance energy transferring to exciton generation). Photocurrent density of the PPy NW device is increased up to 25-fold by Ag NPs attachment under blue light illumination (λ = 425–475 nm), and spectral response of photocurrent is improved in the Ag NPs-decorated PPy NW (PPy_{AgNPs} NW) device. In addition, space charge limited conduction (SCLC) by LSPR is more obviously measured in photocurrent of the devices. The successful demonstration of plasmonic space charge generation of *"metal NPs attached p-type polymer NW"* device can contribute to development of high-performance and inexpensive nano-device fabrication as it can optimize engineering for effective plasmonic coupling in relatively cheap polymer-based nano-devices.

Results and discussion

Figure 1 shows a schematic representation of Ag NPs decoration on PPy NW. The surface of commercial Ag NP is encapsulated by copolymer of polyethylenimine (bPEI) that gives the surface of Ag NPs a positively charged state, while PPy NW has carboxyl group at the surface by using a pyrrole-COOH precursor during electrochemical synthesis of PPy NWs. The Ag NPs can electrostatically attach onto the surface of PPy NWs when the Ag NPs and the PPy NWs are mixed together in a solution. To maximize photon absorption of PPy NWs by LSPR energy transfer of Ag NPs, 80 nm of Ag NPs [Figure 2(c)] were selected because matching or overlapping LSPR with absorption spectrum of the PPy NWs was expected. Figure 2(a) shows the absorption spectra of PPy_{AgNPs} NWs [Figure 2(b)], pristine PPy NWs [Figure 2(d)] and Ag NPs [Figure 2(c)]. The absorption peak of Ag NPs (blue line) represents LSPR in the range of 454–484 nm [$\lambda_{max(1st)}$ = 454 nm, $\lambda_{max(2nd)}$ = 484 nm], which is broader than the absorption peak (472 nm) supplied by the 80 nm of the Ag NPs' vendor. Here, this discrepancy of the absorption peak is regarded as difference due to aggregation of Ag NPs or badge-to-badge. When Ag NPs begin to aggregate and make small clusters, red-shifted spectral peak and broad spectrum are observed due to interaction of their electromagnetic properties in adjacent Ag NPs.[15,16] PPy_{AgNPs} NWs show red-shifted and intensity-increasing absorption peak at 466 nm, differing from that of pristine PPy NWs at 442 nm due to convolution with the absorption spectrum of Ag NPs. The absorption of PPy_{AgNPs} NWs indicates that the LSPR of Ag NPs is strongly reflected in the absorption of PPy_{AgNPs} NWs. Figure 2(b) shows a SEM image of PPy_{AgNPs} NW after dispersion on a substrate. Ag NPs are well adsorbed onto the surface of PPy NW, which implies that LSPR of the Ag NPs can influence absorption of the PPy NW. Attachment of the Ag NPs on PPy NW was double-confirmed by energy-dispersive X-ray spectroscopy (EDS) measurement (Figure S3). In addition, as

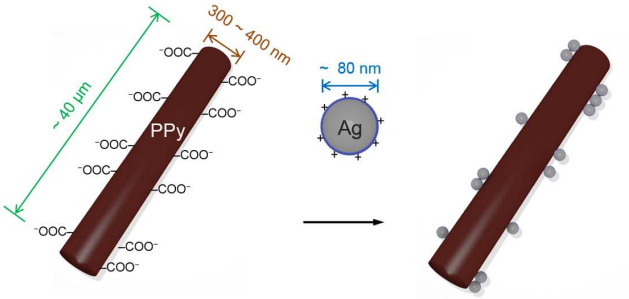

Fig. 1 Schematic diagram of Ag NPs decoration onto PPy NW with electrostatic interaction.

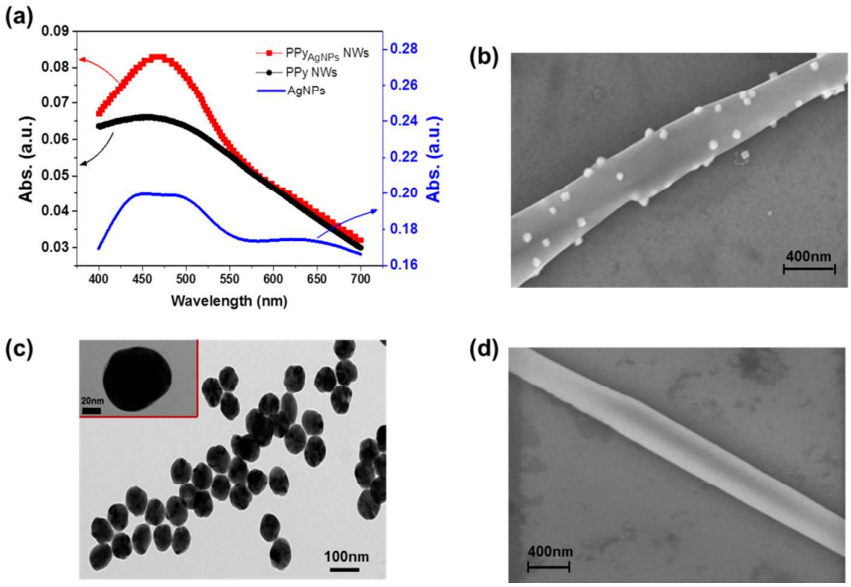

Fig. 2 (a) Absorption spectra of PPy$_{AgNPs}$ NWs, PPy NWs, and Ag NPs. (b) A SEM image of PPy$_{AgNPs}$ NW. (c) A TEM image of the Ag NPs; inset is a TEM image of an individual AgNP. (d) A SEM image of PPy NW.

shown in Figure 2(c) TEM images of the Ag NPs show diameter of Ag NPs at roughly 80 nm and very thin (1–2 nm) bPEI encapsulation. On the other hand, Figure 2(d) shows a SEM image of pristine PPy NW after dispersion on a substrate. Electrostatic force is truly mandatory in the Ag NPs decoration on the PPy NWs; this is confirmed by a control experiment. In case of mixing between the bPEI encapsulated Ag NPs solution and PPy NWs solution without carboxyl group at the surface, the Ag NPs are not attached onto the surface of the PPy NWs (Figure S4). Because the PPy$_{AgNPs}$ NWs show an obvious increase of absorption spectrum, improvement of opto-electric properties can be expected to result from plasmon–exciton coupling between Ag NPs and PPy NWs.

Wavelength-dependent [Red (625 – 675 nm), Green (525 – 575 nm), Blue (425 – 475 nm): RGB] opto-electric properties of individual PPy$_{AgNPs}$ NW and PPy NW devices are comparably demonstrated in Figure 3. To compensate difference by the RGB color-bandpass filtered light intensities in between, intensity-normalized photocurrent density (J^N_{PC}) is obtained: $J^N_{PC} = J_{PC} / I_{RGB} = (J_L - J_D) / I_{RGB,}$ where J_{PC} is photocurrent density, J_L is current density under illumination, J_D is dark current density, and I_{RGB} is light intensity with each bandpass filter. Figure 3(a) and 3(b) display periodical photo-response of PPy$_{AgNPs}$ NW and PPy NW devices under RGB illumination, respectively. J^N_{PC} is measured with 0.1V of bias by applying the RGB color-bandpass filtered light for every other 15 sec, as shown in Figure 3(a) and 3(b). For PPy NW devices, the J^N_{PC} under the periodical blue light illumination is about 2–2.5 orders of magnitude higher than the J^N_{PC} under the periodical red or green light illumination, and the J^N_{PC} levels under the periodical red and green light illuminations are similar to each other [Figure 3(a)]. On the other hand, the PPy$_{AgNPs}$ NW device shows one order of magnitude larger J^N_{PC} than the PPy NW device, as represented in Figure 3(b). In addition, for the PPy$_{AgNPs}$ NW device, the J^N_{PC} under the periodical green light illumination is larger than the J^N_{PC} under the periodical red light illumination. This means that Ag NPs decoration on PPy NW brings about wide spectral response as well as enhancing photocurrent. In order for quantitative characterization, the J^N_{PC} of the PPy$_{AgNPs}$ NW and PPy NW devices at 30 sec (the beginning point of the first illumination "off" state) is displayed in Figure 3(c). The J^N_{PC} of the PPy$_{AgNPs}$ NW and of the PPy NW devices are respectively represented by the solid and hollow bars, and the RGB colors of the bars represent each color of bandpass-filtered light illumination. As shown in Figure 3(c), J^N_{PC} levels are remarkably improved by the decoration of Ag NPs. Efficiency of the improvement (%) can be calculated by $[J^N_{PC}$ (PPy$_{AgNPs}$ NW) – J^N_{PC} (PPy NW)] / J^N_{PC} (PPy NW) × 100. The efficiency of each color bandpass filtered light illumination was increased to 2530% (Blue), 2120% (Green), and 1400% (Red), respectively. The highest efficiency being by blue light results from the effect by LSPR of the Ag NPs, because LSPR of the Ag NPs is maximal at 454–484 nm, as shown in Figure 2(a). In addition, efficiency with the green light is also remarkably high, which is distinguishable from the PPy NW device; J^N_{PC} of the PPy NW shows a remarkable improvement only by the blue light illumination, as shown in Figure 3(a). Therefore, the improvement efficiency (%) of J^N_{PC} in the PPy$_{AgNPs}$ NW device obviously indicates that spectral response of PPy NW device is widened by Ag NPs decoration. The wide spectral response of the PPy$_{AgNPs}$ NW is well matched with the absorption spectrum of PPy$_{AgNPs}$ NWs. The peak in the absorption spectrum of the PPy$_{AgNPs}$ NWs increases and widens, reaching to 550 nm, as shown in Figure 2(a). The wide spectral response of the PPy$_{AgNPs}$ NW can be regarded as due to LSPR of the Ag NPs, similarly to previous reports.[4,11,13]

The remarkably improved J^N_{PC} of PPy$_{AgNPs}$ NWs is certainly related with extending space charge region at the interface by

Ag NPs decoration on PPy NW surface. When Ag NPs are attached on PPy NW surface, band banding at the interface is due to differences in work-function of Ag NPs and fermi level of PPy NW.[14] The band banding at the interface of PPy_{AgNPs} NW means that space charge region is more extended at the surface of PPy_{AgNPs} NW. The extended space charge region can benefit photocurrent enhancement because separation of excitons can be accelerated with enhanced local *E*-field in the space charge region. Therefore, overall J^N_{PC} of PPy_{AgNPs} NWs is notably superior to that of PPy NW as shown in Figure 3(c).

Another interesting behavior observed in the periodical "on–off" photocurrent experiments [Figure 3(a) and 3(b)] is that the J^N_{PC} gradually increases as the "on–off" cycles are repeated; in other words, photocurrent does not fully decay, similarly to darkcurrent, for 15 sec. Such a long photocurrent decay in semiconductors has been frequently reported[17-22] and is generally regarded as indicating that defect-sites play a main role in slow exciton recombination processes.[17,18,22] More interestingly, the PPy_{AgNPs} NW device shows longer photocurrent decay than the PPy NW device. For an obvious characterization, the normalized photocurrent decay in the 1st "on–off" cycle under blue light illumination is represented in Figure 3(d). The cyan and red lines in Figure 3(d) are fitted lines by single exponential equation ($e^{-t/\tau}$). Photocurrent decay time can be characterized by time constant of decay (τ). The τ of PPy_{AgNPs} NW is about 12 sec, twice that of PPy NW (6 sec). The longer decay time can be attributed to extended population and lifetime of photon-excited carriers by the Ag NPs decoration onto the PPy NW. In case of the red and green lights illumination, τ is slightly shorter than the blue light illumination in both cases, as shown in Table 1. Such a dependence of τ on Ag NPs decoration and RGB light illumination is similar to dependence of the J^N_{PC} displayed in Figure 3(a), 3(b), and 3(c). According to previous reports, metals NPs attachment on NW_{Semi} can strengthen the space charge region that behaves like surface defect-sites.[14] As a result the strengthened space charges will make photocurrent decay longer,[3] because defect-sites mainly work on a slow exciton recombination process. The long photocurrent decay associated with Ag NPs decoration observed in this study may be correlated with space charges. Especially, electrochemically fabricated PPy NWs using AAO template used to have non-single crystallinity; therefore, space charges are more favorably generated by structural defects in PPy NWs than single crystallized inorganic NW_{Semi} samples. For example, SCLC is typically reported in bulk and nano-structured PPy samples.[23-26] For that reason, conduction of charge carriers in the PPy NW and PPy_{AgNPs} NW devices has been investigated in detail.

Current density–voltage (*J*–V) characteristics of the devices are represented in Figure 4. Figure 4(a) shows *J*–V curves of the PPy NW and PPy_{AgNPs} NW devices without light illumination (J_{Dark} vs.V); and SEM images of typical PPy NW (left) and PPy_{AgNPs} NW (right) devices are displayed as the insets of Figure 4(a). The J_{Dark}–V curves of the PPy NW and PPy_{AgNPs} NW devices follow a power law ($J_{Dark} \propto V^m$) in the range over 0.3 V, whereas Ohmic behavior is observed in the lower voltage region ($\leq$ 0.1 V) for both devices (Figure S5). The power (*m*) obtained from Figure 4(a) is 2.04 (PPy NW) and 2.31 (PPy_{AgNPs} NW). In case of trap-free (or trap-filled) SCLC, the value of *m* is close to 2, and *m* shows a value larger than 2, if abundant trap-sites exist in the sample.[27] Therefore, the larger *m* is shown in

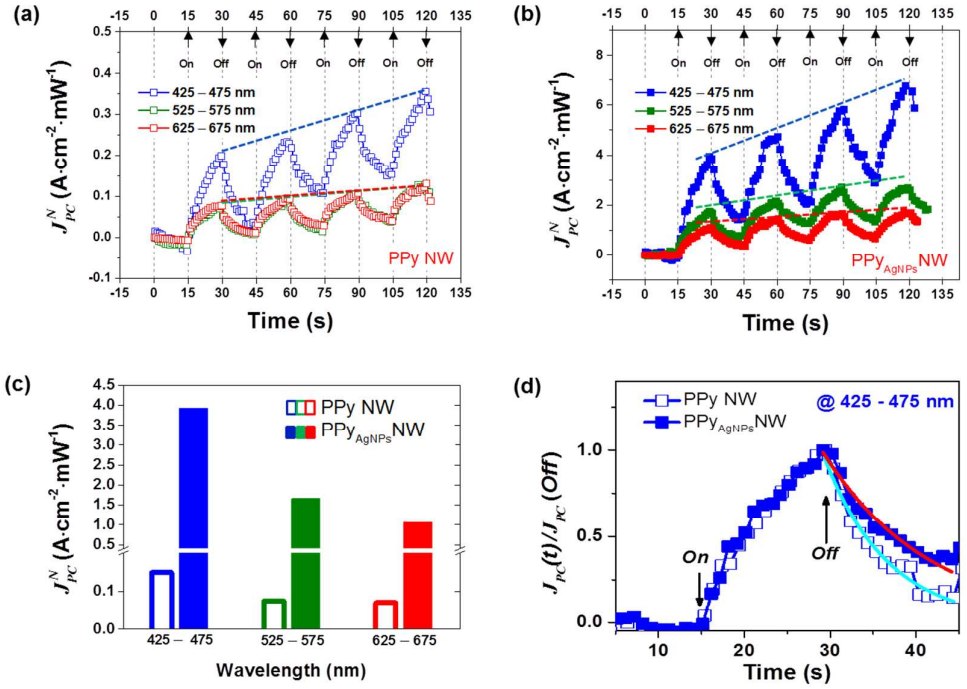

Fig. 3 Periodical RGB-lights illumination-dependent intensity-normalized photocurrent density (J^N_{PC}) of (a) PPy NW and (b) PPy_{AgNPs} NW devices. The colored dashed lines are guides to eyes. (c) Bar graphs of the J^N_{PC} of the PPy NW and PPy_{AgNPs} NW devices obtained at 30 sec in (a) and (b). (d) Normalized photocurrent decay [J_{PC}(t)/J_{PC}(Off)] of the PPy NW and PPy_{AgNPs} NW devices observed in the 1st on–off cycle under the blue light illumination. Solid lines represent single exponential fitting lines.

power law dependence of the *J*–V curve, the more abundant and influential trap-sites like deep-traps can be inferred. The value of *m* increase from 2.04 to 2.31 by decoration of Ag NPs on PPy NW. Space charge region is extended at the interface by decoration of Ag NPs. The enhanced space charge region can shrink the inner conduction channel of PPy NW. Thus, the disturbed charge conduction is similarly reflected as increase of trap-sites (the larger value of *m*), which can be confirmed by the lower current density of PPy_{AgNPs} NW shown in Figure 4(a) and 4(b). Under light illumination, the current density (J_{Light}) shows power law dependence with the slightly smaller value of *m* than the J_{Dark}, as displayed in Figure 4(b). The RGB light dependence of J_{Light} is not clearly distinguishable. The averaged values of *m* for RGB light ($m_{ave.}$) are 1.99 (PPy NW) and 2.26 (PPy_{AgNPs} NW). The value of *m* slightly decreases under the RGB light illumination, which can be interpreted as excitation of trapped charges by irradiating photon energy making an effect likely to decrease number of trap-sites. In order to investigate RGB light dependence on SCLC of the devices carefully, the normalized J^N_{PC} (by J^N_{PC} at 0.3 V) characteristics on V are obtained as shown in Figure 4(c) and 4(d). Only photon-excited charge carriers are reflected in characterization of photocurrent ($J_{PC} = J_{Light} - J_{Dark}$); therefore, wavelength (RGB light) dependent charge conduction could be clearly detectable. For the normalized J^N_{PC} of the PPy NW device [Figure 4(c)], that under blue light illumination has 2.14 of *m*, while the values are 1.40 under red and green light illuminations alike. This means that under blue light illumination the photo-excited charge carriers are more influenced by space charges than under green and red light illuminations, because the values of *m* close to 2 and 1 indicate SCLC and Ohmic conduction, respectively. The maximum absorption (at 442 nm) of the PPy NWs in the blue light region can induce more photo-excited charge carriers; therefore, increasing population of charge carriers could bring about SCLC in the PPy NW device. On the other hand, the normalized J^N_{PC} of the PPy_{AgNPs} NW device has *m* values of 2.70 (Blue), 2.04 (Green), and 1.68 (Red) under RGB light illumination, as shown in Figure 4(d). By the decoration of Ag NPs, space charges are generated more (extending space charge region), which is reflected by the increasing values of *m*. The maximum value of *m* in the PPy_{AgNPs} NW device under blue light illumination indicates that LSPR by the Ag NPs can generate more space charges under blue light illumination. Unlike RGB light dependence of the values of *m* in the PPy NW device, the value of *m*, shown in Figure 4(d), under green light illumination is larger than that under red light illumination. This result closely corresponds with the wide spectral response of the J^N_{PC} by LSPR of the Ag NPs shown in Figure 3(b) and 3(c). Therefore, it seems that the space charges generated by LSPR of the Ag NPs as well as extending space charge region by attachment of the Ag NPs play an important role to improve photocurrent and spectral response of the PPy_{AgNPs} NW device. To clearly demonstrate relation between the degree of space charge generation and the enhanced opto-electrical properties in the devices, all values of *m* (m_{Dark}, m_{Light}, and m_{PC} for J_{Dark}, J_{Light}, and J_{PC}, respectively), photocurrent decay (τ), and the improved photocurrent efficiency by the Ag NPs in the devices are displayed in Table 1. From the RGB light-dependent value of *m* in the PPy_{AgNPs} NW device [Figure 4(d)], degree of space charges generation by LSPR of the attached Ag NPs is supposed to be in order of blue, green, and red light illuminations.

In order to confirm the space charge generation by LSPR of Ag NPs, finite difference time domain (FDTD) simulations on Ag NPs-attached PPy NW were carried out with different

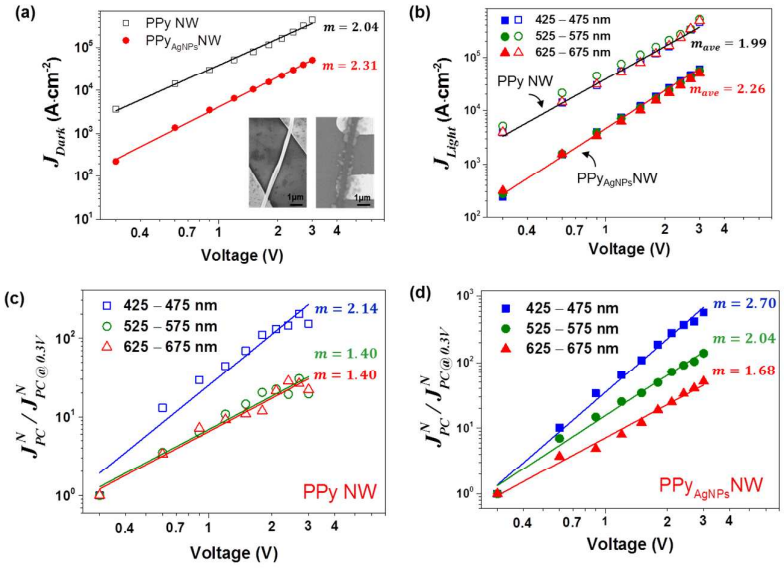

Fig. 4 Graphs of current density and voltage (a) without light illumination (J_{Dark}–V) and (b) with RGB light illumination (J_{Light}–V) of the PPy NW and PPy_{AgNPs} NW (solid) devices. Inset in (a) are SEM images of PPy NW (left) and PPy_{AgNPs} NW (right) devices. (c, d) The normalized J^N_{PC} and voltage characteristics of the (c) PPy NW and (d) PPy_{AgNPs} NW devices. All solid lines represent fitting lines by power law ($J \propto V^m$). The $m_{ave.}$ in (b) is the average of m values of each device under RGB light illumination.

wavelength of electromagnetic (*em*) wave in visible range [Figure 5(a)]. The schematic representation in Figure 5(a) shows configuration of the FDTD simulation; a monitor [14.5 nm (*x*) × 80 nm (*y*)] is placed near the interface between a single Ag NP and a PPy NW, and a plane *em* wave is set-up to inlet from the bottom of the NW by putting with the magnetic field component (*H*-field) of the *em* wave along with the NW (TE mode). Distributions of *E*-field intensity (E^2) in the monitor area at certain wavelengths (representing RGB) of the *em* wave are represented as the contour plots in Figure 5(b). For ease of recognition, average of E^2 at the interface area (the black hollow box representatively shown in the contour plot of 430 nm) in the monitor is obtained and displayed as the white-colored numbers in each contour plots. High intensity of E^2 can be induced when charges are localized (space charges). Maximum of the average of E^2 (294 V^2m^{-2}) is obtained with 430 nm of *em* wave irradiation, and the average of E^2 decreases in the order of 450 nm (228 V^2m^{-2}), 550 nm (135 V^2m^{-2}), and 650 nm (121 V^2m^{-2}). This means that space charges are most strongly generated under the blue light illumination (425–475 nm) and that the space charge generation decreases in the order of the green (525–575 nm) and red (625–675 nm) light illuminations. Especially, E^2 is locally strong at the interface of the Ag NP, as well as the distribution of E^2 reaching more deeply inside of the NW under the blue light illumination than the others reach. This result is well matched with the dependence of the *m* obtained in the *J*–V characteristics (Figure 4). Both the *J*–V characteristics and the FDTD simulation obviously prove that space charges can be generated at the interface between Ag NP and PPy NW by LSPR of the Ag NP.

As further evidence of SCLC in the PPy_{AgNPs} NW and PPy NW devices, intensity dependence of photocurrent gain (Γ) is also characterized, as shown in Figure 5(b). In general, Γ represents the ratio between the number of generated charges and the number of the in-letting photons as the following equation:[28, 29] $\Gamma = (i_{PC}/q)/(P/h\nu) \times 1/\eta$, where i_{PC} is photocurrent, q is the electron charge, P is the power of absorbed photon into sample, $h\nu$ is the irradiating photon energy, and η is the quantum efficiency. In the present characterization, η is simply regarded as 1, and P is obtained by multiplication of illuminated light intensity (I) and geometrical factors (length: l, diameter: ϕ) of the NWs: $I \times l \times \phi$. Moreover, summations of photon energy and power ($h\nu$ and I) in the range of 425–475 nm are complementally used owing to the broad spectrum of the light source. The intensity (*x*-axis) of the graph in Figure 5(c) represents measured intensity of the illuminated light source at 450 nm. As shown in Figure 5(c), the photocurrent gain by the blue light illumination (Γ_{Blue}) shows inverse power law dependence with intensity of the illuminated light source ($\Gamma_{Blue} \propto I^{-\kappa}$). The values of exponent κ are 0.85 ± 0.03 (PPy_{AgNPs} NW) and 0.71 ± 0.02 (PPy NW). According to the previous reported simulation[20] and experimental[14] studies, if space charge regions exist near the surface of the sample and can modulate photocurrent conduction, κ has a value between 0.5 and 0.9 as well as inverse power law dependence with I in typical conditions. Therefore, the dependence of Γ_{Blue} shown in Figure 5(c) is corresponds strongly to the aforementioned data related with plasmonic space charge generation. In addition, the Γ_{Blue} is improved approximately 2-fold by decoration of Ag NPs; a similar degree of improvement of Γ has been reported in NW_{semi} devices with extending space charge regions by

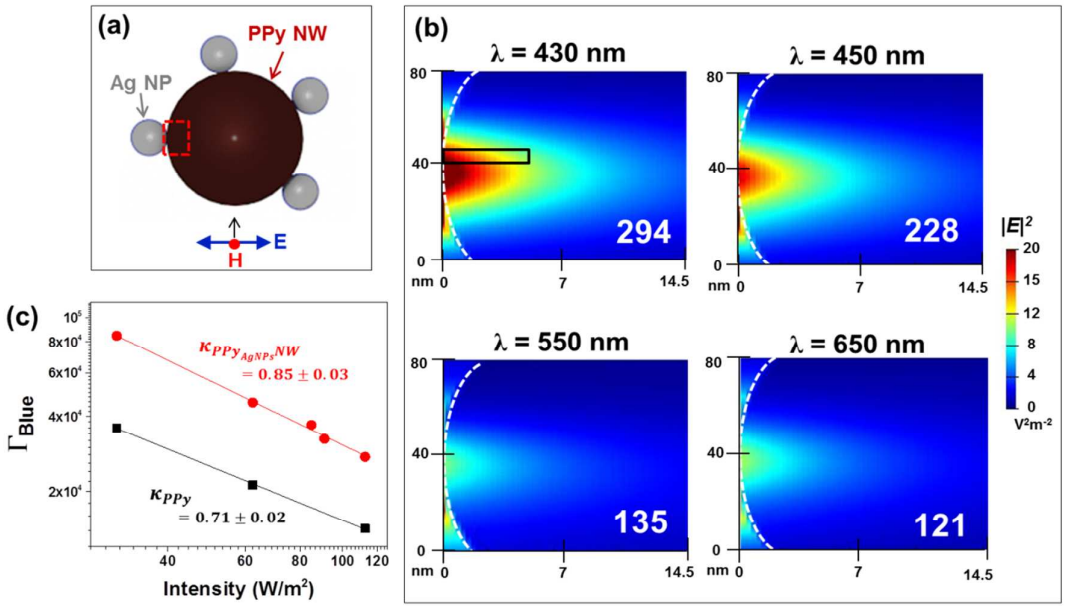

Fig. 5 (a) Schematic representation of Ag NPs decorated PPy NW for FDTD simulation with the plane *em*-wave source (TE mode with the PPy NW). Propagating direction of the *em*-wave source is displayed by the black arrow. (b) Contour plots of *E*-field intensity (E^2) are measured in the interface [the red dashed box in (a)] between Ag NP and PPy NW with 430 nm, 450 nm, 550 nm, and 650 nm wavelengths of the source. The white colored numbers represent the average of E^2 in the specific area in the contour plots; the specific area is displayed as the black hollow box in the contour plot of 430 nm, and the average of E^2 of the other contour plots are measured in the same area as the contour plot of 430 nm. The white dashed lines represent surface of the PPy NW. (c) Intensity of the blue light-dependent photocurrent gain (Γ_{Blue}) of PPy NW and PPy_{AgNPs} NW devices. Solid lines are fitted lines with power law ($\Gamma_{Blue} \propto I^{-\kappa}$).

attachment of NPs.[3,14,30]

Parameter	m_{Dark}	m_{Light} (Blue) (Green) (Red)	m_{PC}	τ, Sec.	Efficiency of improvement,%
PPy NW	2.04	1.99 (2.02) (1.91) (2.03)	2.14 (Blue) 1.40 (Green) 1.40 (Red)	6.2 (Blue) 5.0 (Green) 5.6 (Red)	N/A
$PPy_{Ag\ NPs}$NW	2.31	2.26 (2.35) (2.26) (2.17)	2.70 (Blue) 2.04 (Green) 1.68 (Red)	12.0 (Blue) 11.7 (Green) 11.6 (Red)	2530 (Blue) 2120 (Green) 1400 (Red)

Table 1 Major parameters of PPy NW and PPy_{AgNPs} NW devices. The m_{Dark}, m_{Light}, and m_{PC} are exponents obtained from J_{Dark}, J_{Light}, and the normalized J^{N}_{PC} shown in Figure 4, respectively. For m_{Light}, average and individual values under RGB light illumination are displayed together. The time constant of photocurrent decay (τ) and efficiency of improvement are obtained from Figure 3.

Based upon the experimental and simulation results, the mechanism of enhanced photocurrent by plasmonic space charge generation in PPy_{AgNPs} NW is proposed in Figure 6. Figure 6(a) represents schematic illustration and energy band diagrams of Ag NP and PPy NW before attachment. Fermi energy (E_F) of Ag NP is decided as 4.26 eV due to E_F of bulk Ag.[31] Conduction band energy (E_C) and valance band energy (E_V) of PPy NW are adopted from the literature.[32] Because PPy is a typical *p*-type conducting polymer, the majority of carriers will have positive charge (considered as "hole" in Figure 6) and E_F of PPy is placed near E_V. Moreover, trap energy (E_t) levels possibly exist near the surface of PPy NW due to surface defect-sites of PPy NW; the existence of E_t levels can be inferred from SCLC behavior of the PPy NW device. Because E_F of Ag NP (4.26 eV) is much smaller than E_F of PPy NW (~ 6.1 eV), electrons of Ag NP are able to transform to PPy NW when Ag NP is attached on the surface of PPy NW [Figure 6(b)].[33,34] The band diagram of Figure 6(b) shows that Ag NP works as an electron donor-like surface state, and depletion region (from the point of view of the hole) definitely forms at the interface between AgNP and PPy NW. As shown in the schematic illustration of Figure 6(b), the depletion region generated by Ag NP will hamper transport of PPy NW; this situation can be indicated by the smaller m_{Dark} and larger J_{Dark} of the PPy NW than those of the PPy_{AgNPs} NW, as shown in Figure 4(a). Under the red light illumination on the Ag NP attached PPy NW [Figure 6(c)], bandgap of PPy NW is sufficiently large not to generate exciton; however, the defect-sites can be filled with electrons generated by the photon energy (1.84–1.98 eV). On the other hand, photon-generated holes are not localized by the E_t levels; therefore, hole population relatively increases in the depletion region under the red light illumination. Increasing hole population will depress the depletion region, so that the transport in the Ag NP-attached PPy NW is somehow discharged by the shrunk depletion region, as shown in the schematic illustration of Figure 6(c); this can be inferred by the smaller m_{Light} *(Red)* (2.17) than m_{Dark} (2.31) in the PPy_{AgNPs} NW device as shown in Table 1. In case of blue light illumination, strong LSPR is induced at the surface of Ag NP [Figure 6(d)]. Hot-electrons generated by the LSPR enter into the interface of PPy NW. In addition, excitons are most effectively generated in PPy NW under blue light illumination; thus, electrons from the excitons can move to the lower band in the depletion region. In the result, population of electrons increases in the depletion region; therefore, the depletion region is extended as show in Figure 6(d). The extended depletion region can further hamper the transport in the Ag NP attached PPy NW, which is reflected by the larger m_{Light} *(Blue)* (2.35) of the PPy_{AgNPs} NW device, as displayed in Table 1. According to the absorption spectra of the Ag NPs and PPy_{AgNPs} NWs shown in Figure 2(a), LSPR of the Ag NPs can be expected under green light illumination. Thus, a similar but less effective situation to that under blue light illumination [Figure 6(d)] will exist under green light illumination.

The suggested mechanism in Figure 6 is helpful to understand the correlation between variation of space charges and enhancement of photocurrent in PPy_{AgNPs} NW. According to the mechanism, the accumulated electrons in the depletion region bring about SCLC in the NW due to restriction of transport of charge carriers, and the accumulated electrons can be regarded as space charges. Increasing space charges locally enhance *E*-field; therefore, excitons effectively separated by the locally enhanced *E*-field can improve photocurrent in the NW. For the red light illumination, although the depletion region decreases, the non-localized photon-generated holes can deploy to enlarge the photocurrent. In the case of blue light illumination, *E*-field can be more effectively enhanced by hot-electrons generated by LSPR of AgNP. Moreover, excitons are most effectively generated with maximum absorption of PPy NW. In addition, owing to resonance photon scattering or plasmon resonance

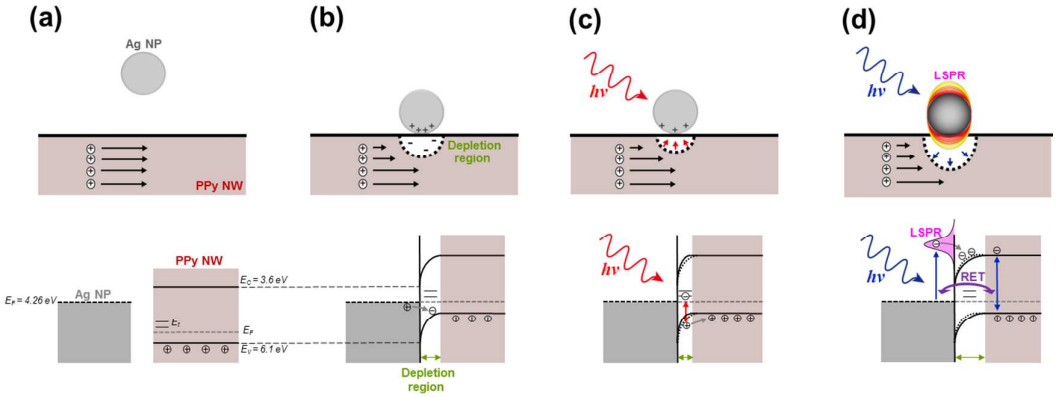

Fig. 6 Schematic illustration (above) and energy band diagrams (below) of Ag NP and PPy NW (a) before and (b) after attachment, under (c) red and (d) blue light illumination. "LSPR" and "RET" in (d) represent localized surface plasmon resonance and resonance energy transfer, respectively.

energy transfer between the LSPR of the Ag NP and photon absorption of the PPy NW, hot-electron injection and exciton generation would be accelerated. Thus, remarkably enhanced photocurrent is available in the PPy_{AgNPs} NW under blue light illumination.

Conclusions

By means of metal particle decoration, opto-electrical properties of p-type non-single crystallized NWSemi device are successfully improved. The electrostatical attachment of Ag NPs onto PPy NW surface has resulted in distinct plasmonic space charge generation under the blue light illumination, which has been ascertained by both experimental J–V characterization and FDTD simulation. The plasmonic space charges play an important role in enhancing photocurrent efficiency, spectral response, and photocurrent decay in the PPyAgNPs NW device; the plasmonic space charges extend the depletion region at the interface of the PPyAgNPs NW and enhancing local E-field to accelerate separation of exciton effectively (enhancing photocurrent). Moreover, owing to matching between LSPR of the Ag NPs and photon absorption of the PPy NW, exciton generation and separation have synergistically worked for enhancement of photocurrent. In the result, remarkably high photocurrent efficiency (2530%) of the PPyAgNPs NW device under the blue light illumination and wide spectral response (high photocurrent response by the green light as well as the blue light illuminations) is achieved in the PPyAgNPs NW device. The present results successfully demonstrate that the previously reported LSPR effect by metal NP decoration on n-type NWsemi device can be applied with a typical p-type non-single crystallized polymer NW device, too. In particular, combination between metal NP (work function) and polymer NW (energy levels) is an important factor to form depletion region at the interface of p-type NWsemi device. Furthermore, it turns out again that utilizing plasmon–exciton coupling (matching between LSPR of metal NPs and absorption of polymer NW) is an effective way to enhance opto-electric properties in the sample system. These results can help optimize engineering in applications of relatively cheap polymer-based functional nano-devices, and also benefit understanding for enhanced photoactivity by increased charge separation by metal deposition.

Experimental

Sample preparation

Carboxyl group-modified PPy NW is fabricated by an electrochemical method with anodic aluminum oxide (AAO) template. The fabrication of the carboxyl group-modified PPy NWs was carried out by applying 1200 mV and 10 mA for 30 min to the AAO template in 10 mL of acetonitrile solution with 1H-pyrrole-1-propionic acid (0.5 M) and $LiClO_4$ (0.2 M). After the electrodeposition of PPy NWs, the AAO template was removed using 3M of NaOH. Length and diameter of the fabricated PPy NWs are over 20 μm and 300–400 nm, respectively (Figure S1). Positive charge-modified Ag NPs were purchased from nanoComposix Inc. The positively charged Ag NPs aqueous solution (0.005 mM, 0.4 μl) was added to the negatively charged PPy NWs aqueous solution (0.5 mM, 0.4 μl), then the blended Ag NPs and PPy NWs solution was stirred for 30 min, in order to electrostatically attach the Ag NPs on the PPy NWs. After stirring, the excessive Ag NPs were removed by several sequential centrifuging and rinsing processes. The solution of PPy_{AgNPs} NWs was drop-casted on an Au micro-electrode chip for opto-electrical measurement, as shown in Figure S2. For the control experiment, PPy NW devices were also prepared in the same manner as the PPy_{AgNPs} NW device (Figure S2).

Opto-electrical characteristic

Voltage–current (V–I) characteristics of the PPy NW and PPy_{AgNPs} NW devices were measured by using a sourcemeter (Keithley 2400). For wavelength-dependent photocurrent measurement, a halogen lamp (150 W, SOL-R DR, Fiberoptics Technology Inc.) with broad bandpass interference filters (425–475 nm, 525–575 nm, and 625–675 nm, Edmund optics.) were used as the light source. The intensity of the band-passed light irradiations was measured at the sample position by a calibrated silicon photodetector (Newport 818-UV/DB) at 450 nm, 550 nm, and 650 nm. For the comparison of the NW devices, measured photocurrents were carefully normalized with the light intensity and dimension of the NWs (See *Supporting Information*). For the "on–off" photocurrent experiment (3 V is applied), the light path between the light source and the sample stage was periodically (30 sec intervals) blocked for 15 sec by an insulating and non-transparent plate. V–I measurements were carried out with minimal contact resistances.[35] Measurements of photocurrent gain were carried out by a light source using the halogen lamp with the blue-color bandpass filter (425–475 nm). The intensity of the light source was controlled by changing the lamp power, and photocurrent was measured immediately after the light irradiation.

FDTD Simulations

E-field intensity in PPy_{AgNPs} NW dependent on wavelength of light irradiation was measured using a 3-dimensional FDTD simulation tool (Lumericals Inc.). Diameters of Ag NPs and PPy NW were set as 80 nm and 400 nm, respectively. In order to consider positively charged polymer layer on surface of the Ag NPs, a 2 nm gap between the Ag NP and PPy NW was set. In the simulation, only single Ag NPs attachment on PPy NW is considered. The FDTD simulations were carried out with total-field scattered field (TFSF) source.

Absorption measurement

Absorption spectra of the Ag NPs and the PPy NWs were measured by using Ag NPs aqueous solution (0.005 mM, 0.4 μl) and PPy NWs aqueous solution (0.5 mM, 0.4 μl), respectively.

Measurements of absorption spectrum of the PPy_{AgNPs} NWs were sequentially conducted by using a mixed solution of the Ag NPs and the PPy NW aqueous solution. The measurements of the absorption spectra were carried out with UV-VIS-NIR spectrometers (JASCO V-550 and JASCO V-670).

Electron microscopy

All images of Scanning Electron Microscopy (SEM) images were obtained using field emission scanning electron microscopes (ZEISS Supra 40VP, JEOL JSM-6700F). Transmission Electron Microscopy (TEM) (JEOL JEM-2100F) was carried out to characterize geometry of the positively charged Ag NPs (Figure 2c).

Acknowledgements

This research was supported by Basic Science Research Program through the National Research Foundation of Korea (NRF) funded by the Ministry of Education, Science and Technology (No. 2013K1A3A1A32035429 and 2015R1A1A1A05027681).

References

1 P. Fan, U. K. Chettiar, L. Cao, F. Afshinmanesh, N. Engheta and M. L. Brongersma, *Nat. Photonics*, 2012, **6**, 380-385.
2 B. P. Khanal, A. Pandey, L. Li, Q. Lin, W. K. Bae, H. Luo, V. I. Klimov and J. M. Pietryga, *ACS Nano*, 2012, **6**, 3832-3840.
3 M.-L. Lu, C.-W. Lai, H.-J. Pan, C.-T. Chen, P.-T. Chou and Y.-F. Chen, *Nano Lett.*, 2013, **13**, 1920-1927.
4 K. Wu, W. E. Rodriguez-Cordoba, Y. Yang and T. Lian, *Nano Lett.*, 2013, **13**, 5255-5263.
5 S. Linic, P. Christopher and D. B. Ingram, *Nat. Mater.*, 2011, **10**, 911-921.
6 J. K. Hyun and L. J. Lauhon, *Nano Lett.*, 2011, **11**, 2731-2734.
7 I. Thomann, B. A. Pinaud, Z. Chen, B. M. Clemens, T. F. Jaramillo and M. L. Brongersma, *Nano Lett.*, 2011, **11**, 3440-3446.
8 H. Gao, C. Liu, H. E. Jeong and P. Yang, *ACS Nano*, 2012, **6**, 234-240.
9 H. M. Chen, C. K. Chen, C.-J. Chen, L.-C. Cheng, P. C. Wu, B. H. Cheng, Y. Z. Ho, M. L. Tseng, Y.-Y. Hsu, T.-S. Chan, J.-F. Lee, R.-S. Liu and D. P. Tsai, *ACS Nano*, 2012, **6**, 7362-7372.
10 Z. Zhang, L. Zhang, M. N. Hedhili, H. Zhang and P. Wang, *Nano Lett.*, 2013, **13**, 14-20.
11 Y.-C. Pu, G. Wang, K.-D. Chang, Y. Ling, Y.-K. Lin, B. C. Fitzmorris, C.-M. Liu, X. Lu, Y. Tong, J. Z. Zhang, Y.-J. Hsu and Y. Li, *Nano Lett.*, 2013, **13**, 3817-3823.
12 H. Yoo, C. Bae, Y. Yang, S. Lee, M. Kim, H. Kim, Y. Kim and H. Shin, *Nano Lett.*, 2014, **14**, 4413-4417.
13 A. Pescaglini, A. Martín, D. Cammi, G. Juska, C. Ronning, E. Pelucchi and D. Iacopino, *Nano Lett.*, 2014, **14**, 6202-6209.
14 C.-H. Lin, T.-T. Chen and Y.-F. Chen, *Opt. Express*, 2008, **16**, 16916-16922.
15 V. Chegel, O. Rachkov, A. Lopatynskyi, S. Ishihara, I. Yanchuk, Y. Nemoto, J. P. Hill and K. Ariga, *J. Phys. Chem. C*, 2012, **116**, 2683-2690.
16 K.-C. Lee, S.-J. Lin, C.-H. Lin, C.-S. Tsai and Y.-J. Lu, *Surf. Coat. Technol.*, 2008, **202**, 5339-5342.
17 R. Calarco, M. Marso, T. Richter, A. I. Aykanat, R. Meijers, A. Hart, T. Stoica and H. Lueth, *Nano Lett.*, 2005, **5**, 981-984.
18 H.-Y. Chen, R.-S. Chen, N. K. Rajan, F.-C. Chang, L.-C. Chen, K.-H. Chen, Y.-J. Yang and M. A. Reed, *Phys. Rev. B*, 2011, **84**, 205443.
19 E. Frankevich, A. Zakhidov, K. Yoshino, Y. Maruyama and K. Yakushi, *Phys. Rev. B*, 1996, **53**, 4498-4508.
20 J. A. Garrido, E. Monroy, I. Izpura and E. Muñoz, *Semicond. Sci. Technol.*, 1998, **13**, 563.
21 C. H. Lee, G. Yu and A. J. Heeger, *Phys. Rev. B*, 1993, **47**, 15543-15553.
22 K. W. Lee, H. H. Mo, i.-m. Kim and C.-E. Lee, *Solid State Commun.*, 2005, **136**, 63-66.
23 W. Bantikassegn and O. Inganaes, *J. Phys. D: Appl. Phys.*, 1996, **29**, 2971-2975.
24 R. Valaski, S. Ayoub, L. Micaroni and I. A. Hummelgen, *Thin Solid Films*, 2002, **415**, 206-210.
25 P. Anjaneyulu, C. S. S. Sangeeth and R. Menon, *J. Appl. Phys.*, 2010, **107**, 093716/093711-093716/093716.
26 S. Biswas, B. Dutta and S. Bhattacharya, *J. Appl. Phys.*, 2013, **114**, 143701/143701-143701/143711.
27 K. C. Kao and W. Hwang, Electrical transport in solids (International series in the science of the solid state), 1987.
28 R.-S. Chen, H.-Y. Chen, C.-Y. Lu, K.-H. Chen, C.-P. Chen, L.-C. Chen and Y.-J. Yang, *Appl. Phys. Lett.*, 2007, **91**, 223106.
29 M. Razeghi and A. Rogalski, *J. Appl. Phys.*, 1996, **79**, 7433-7473.
30 M.-L. Lu, T.-Y. Lin, T.-M. Weng and Y.-F. Chen, *Opt. Express*, 2011, **19**, 16266-16272.
31 M. Uda, A. Nakamura, T. Yamamoto and Y. Fujimoto, *J. Electron. Spectrosc. Relat. Phenom.*, 1998, **88–91**, 643-648.
32 Z. Wang, P. Xiao, L. Qiao, X. Meng, Y. Zhang, X. Li and F. Yang, *Physica B*, 2013, **419**, 51-56.
33 Z. Zhang and J. T. Yates, *Chem. Rev.*, 2012, **112**, 5520-5551.
34 P. B. Weisz, *J. Chem. Phys*, 1953, **21**, 1531-1538.
35 S.-H. Lee, J. Bae, S. W. Lee and J.-W. Jang, *Bull. Korean Chem. Soc.*, 2014, **35**, 2415-2418.